Supporting Information for "Siege of the South: Hunga Tonga-Hunga Ha'apai Water Vapor Excluded from 2022 Antarctic Stratospheric Polar Vortex"

Gloria L. Manney[1,2], Michelle L. Santee[3], Alyn Lambert[3], Luis F. Millán[3], Ken Minschwaner[2], Frank Werner[3], Zachary D. Lawrence[4,5], William G. Read[3], Nathaniel J. Livesey[3], Tao Wang[3]

[1]NorthWest Research Associates, Socorro, NM, USA

[2]New Mexico Institute of Mining and Technology, Socorro, NM, USA

[3]Jet Propulsion Laboratory, California Institute of Technology, Pasadena, CA, USA

[4]Cooperative Institute for Research in Environmental Sciences (CIRES) & NOAA Physical Sciences Laboratory (PSL), University of Colorado, Boulder, Colorado, USA.

[5]NorthWest Research Associates, Boulder, CO, USA

Contents of this file

1. Figures S1 to S12

Corresponding author: Gloria L Manney, NorthWest Research Associates & New Mexico Institute of Mining and Technology, Department of Physics, 333 Workman, Socorro, NM 87801, USA. (manney@nwra.com)

Introduction

This file contains supplementary figures for "Siege of the South: Hunga Tonga-Hunga Ha'apai Water Vapor Excluded from 2022 Antarctic Stratospheric Polar Vortex".

Figures S1 and S2 show full-mission equivalent latitude (EqL) time series of the MLS fields shown in Figs. 1 and 2 in the main text, confirming the uniqueness of the extravortex HTHH signature in H_2O and the ordinariness of the evolution of all species within the stratospheric polar vortex. Fig. S3 presents Aura mission-long EqL/time plots at 380 K, showing only MLS species that have scientifically useful data at pressures of 215 hPa or above (since much of the 380 K surface is at pressures near or above that level), confirming that composition was not unusual in 2022 at subvortex levels. Figures S1 through S3 also include anomalies in two indicators of mixing, effective diffusivity (K_{eff}) and PV gradients. The years 2020 through 2022 all show relatively high PV gradient anomalies and low K_{eff} anomalies near the vortex edge in late winter and spring at all levels, consistent with the long-lived polar vortices in these years; other years during the Aura mission, including 2006, 2010, 2011, and 2015, show similar features, also generally related to long-lived polar vortices.

Figure S4 shows anomalies from the 2005–2021 climatology of vortex-averaged diabatic descent rates from MERRA-2 (note that stronger descent, that is, more negative values, is shown in red for emphasis), demonstrating that descent rates in the middle stratospheric vortex in late winter/early spring 2022 were smaller than usual (consistent, to first order, with lower vortex temperatures) but no more so than in several other years during the Aura mission. This is in contrast to large changes in descent in mid-latitudes (e.g., Coy et al., 2022).

Figures S5 through S7 show EqL/θ snapshots like those in Fig. 3 in the main text, but for 2018, 2020, and 2021 (a near-average year and two unusually cold years with larger-than-usual Antarctic "ozone holes"). Comparing these with Fig. 3 emphasizes that vortex conditions in 2022 were not extreme at any point during the season.

Figures S8 and S9 show profiles summarizing the evolution of dynamical diagnostics and trace gases presented in Fig. 4 in the main text. None of the vortex diagnostics (Fig. S8) show 2022 as the most extreme year in the 43-year MERRA-2 record at any level. Several of those maxima, especially related to vortex and polar processing potential duration, were redefined in 2020. 2021 also had an unusually strong and persistent lower stratospheric vortex, as did 2022, but there were previous years with stronger or more persistent vortices than each of these years. The MLS measurements (Fig. S9) emphasize clearly the near-average nature of the trace gas evolution in the vortex in 2022 from subvortex levels (the lower limit of the profiles shown is 370 K) to the upper stratosphere, consistent with the time series at selected levels shown in Fig. 4 in the main text. In particular, ClO was lower and lower-stratospheric O_3 higher in spring (October/November) 2022 than in 2020, 2021, and several other years also characterized by cold long-lived polar vortices.

As shown in Fig. 5 in the main text, scatter plots of H_2O with long-lived transport tracers demonstrate the separation of the HTHH enhancement from high H_2O that may descend inside the stratospheric polar vortex. Figure S10 shows the relationship between H_2O and CO in the middle stratosphere in the same way that Fig. 5 shows its relationship with N_2O. The results confirm the separation by the vortex edge transport barrier of air with high H_2O and low CO in the HTHH plume from air with high H_2O and high CO that descends inside the polar vortex.

Measurements from the Atmospheric Chemistry Experiment-Fourier Transform Spectrometer (ACE-FTS) also show the distinction between and separation from vortex air of the HTHH H_2O. Version 4.1/4.2 ACE-FTS data are used here, along with corresponding error flags (Boone et al., 2020; Sheese et al., 2022). Figure S11 shows mission-long ACE-FTS measurements of H_2O and the HDO / H_2O ratio (ΔD) at 700 and 550 K. The unprecedentedly high extravortex values of ΔD associated with the high H_2O demark the HTHH plume, since the seawater injected by HTHH has a higher isotope ratio (e.g., Randel et al., 2012; Khaykin et al., 2022, and references therein). ΔD generally increases with height and latitude in the stratosphere, similar to age of air (Randel et al., 2012), hence the larger values in the polar vortex. While ACE-FTS has coverage of much of the Antarctic polar vortex only in July–September, Figure S12 shows that during that time period, the high ΔD values in the HTHH plume are clearly separated from the high values in the polar vortex, with the latter generally occurring at lower H_2O values.

References

Boone, C., Bernath, P., Cok, D., Jones, S., & Steffen, J. (2020). Version 4 retrievals for the atmospheric chemistry experiment Fourier transform spectrometer (ACE-FTS) and imagers. *Journal of Quantitative Spectroscopy and Radiative Transfer*, *247*, 106939. Retrieved from https://www.sciencedirect.com/science/article/pii/S0022407319305916 doi: https://doi.org/10.1016/j.jqsrt.2020.106939

Coy, L., Newman, P. A., Wargan, K., Partyka, G., Strahan, S. E., & Pawson, S. (2022). Stratospheric Circulation Changes Associated With the Hunga Tonga-Hunga Ha'apai Eruption. *Geophysical Research Letters*, *49*(22), e2022GL100982. Retrieved 2022-11-27, from https://onlinelibrary.wiley.com/doi/abs/10.1029/2022GL100982

(_eprint: https://onlinelibrary.wiley.com/doi/pdf/10.1029/2022GL100982) doi: 10.1029/2022GL100982

Khaykin, S., Podglajen, A., Ploeger, F., Grooß, J.-U., Tence, F., Bekki, S., ... Ravetta, F. (2022, December). Global perturbation of stratospheric water and aerosol burden by Hunga eruption. *Communications Earth & Environment*, *3*(1), 316. Retrieved from https://doi.org/10.1038/s43247-022-00652-x

Randel, W. J., Moyer, E., Park, M., Jensen, E., Bernath, P., Walker, K., & Boone, C. (2012). Global variations of HDO and HDO/H2O ratios in the upper troposphere and lower stratosphere derived from ACE-FTS satellite measurements. *Journal of Geophysical Research: Atmospheres*, *117*(D6). Retrieved from https://agupubs.onlinelibrary.wiley.com/doi/abs/10.1029/2011JD016632 doi: https://doi.org/10.1029/2011JD016632

Sheese, P. E., Walker, K. A., Boone, C. D., Bourassa, A. E., Degenstein, D. A., Froidevaux, L., ... Zou, J. (2022). Assessment of the quality of ACE-FTS stratospheric ozone data. *Atmospheric Measurement Techniques*, *15*(5), 1233–1249. Retrieved from https://amt.copernicus.org/articles/15/1233/2022/ doi: 10.5194/amt-15-1233-2022

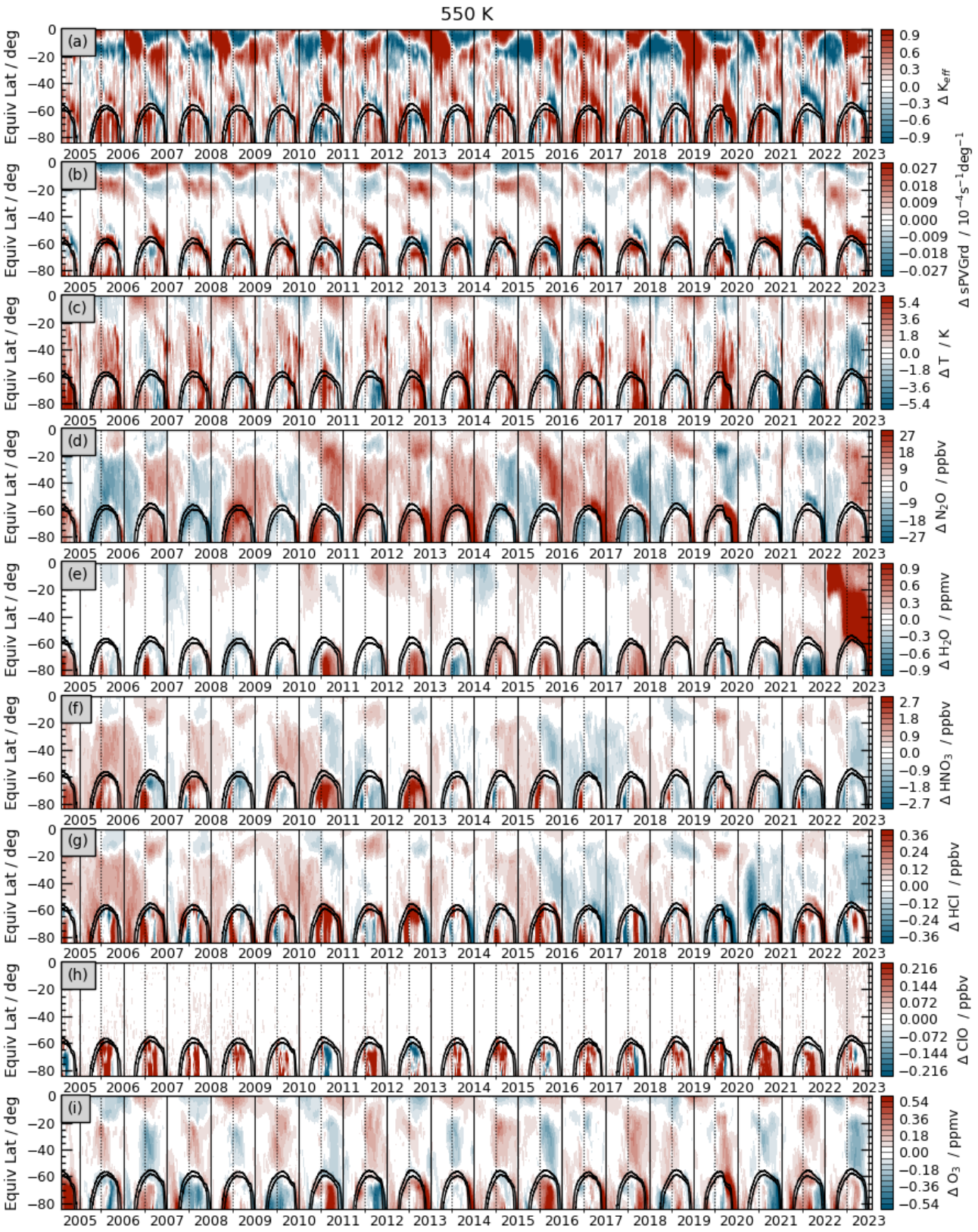

Figure S1. SH equivalent latitude / time series at 550 K of anomalies from the 2005–2021 climatology of (top to bottom) MERRA-2 effective diffusivity (K_{eff}) and sPV gradients and MLS temperature, N_2O, H_2O, HNO_3, HCl, ClO, and O_3, shown for the full Aura mission through January 2023. Black overlays are sPV contours indicating the vortex edge region.

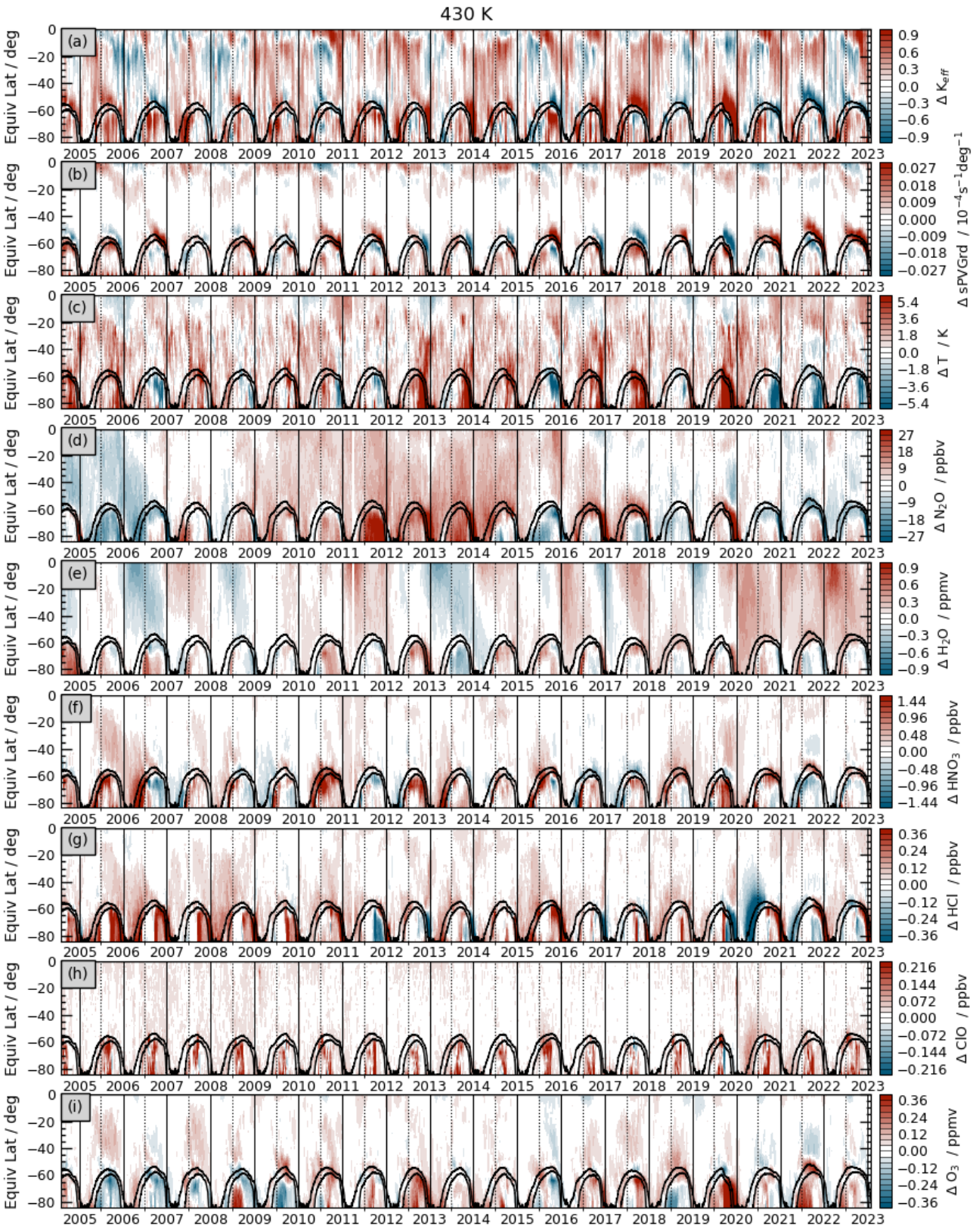

Figure S2. As in Fig. S1 but at 430 K.

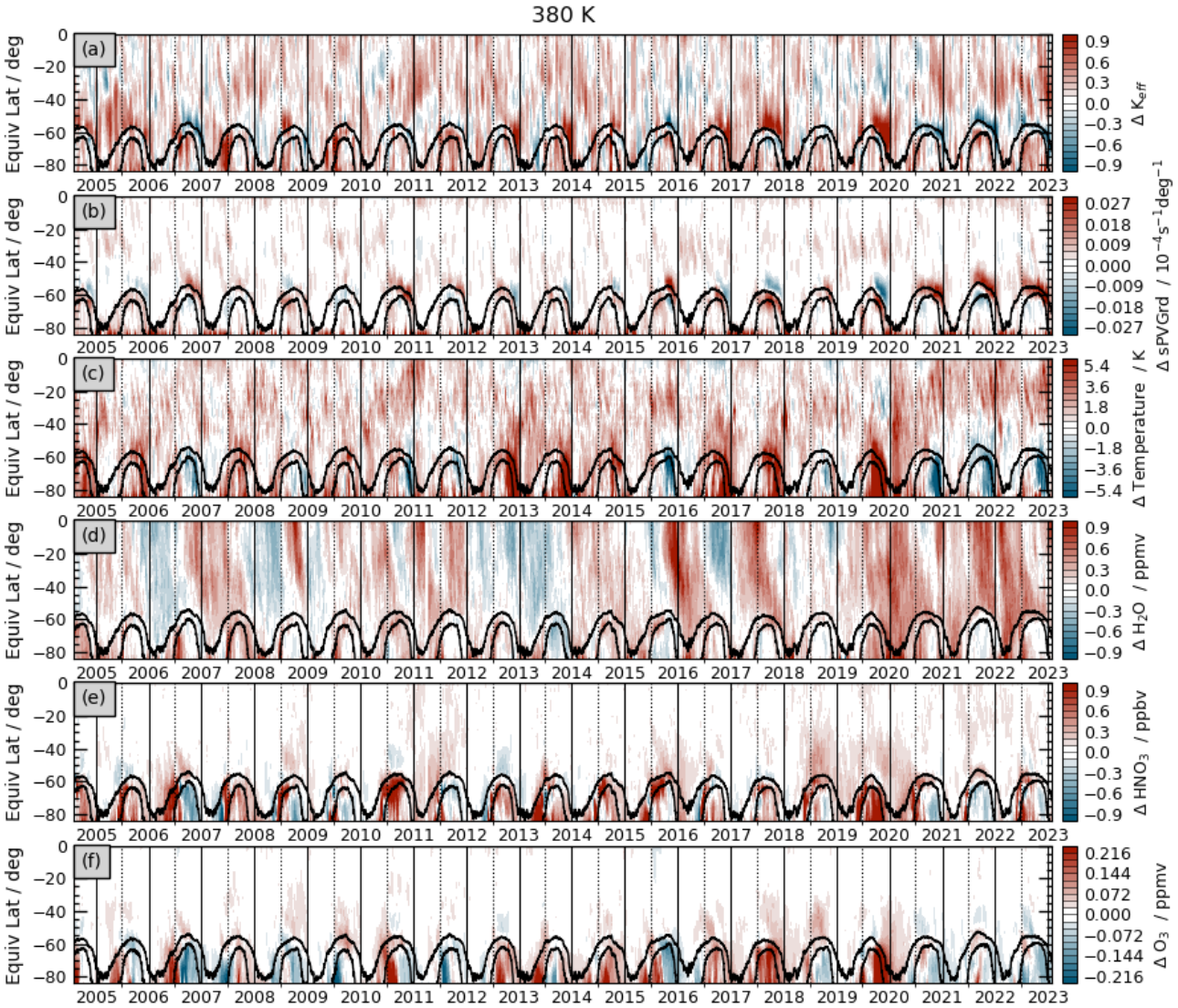

Figure S3. As in Fig. S1, but for 380 K and showing only MLS species with scientifically useful data at 215 hPa and larger pressures.

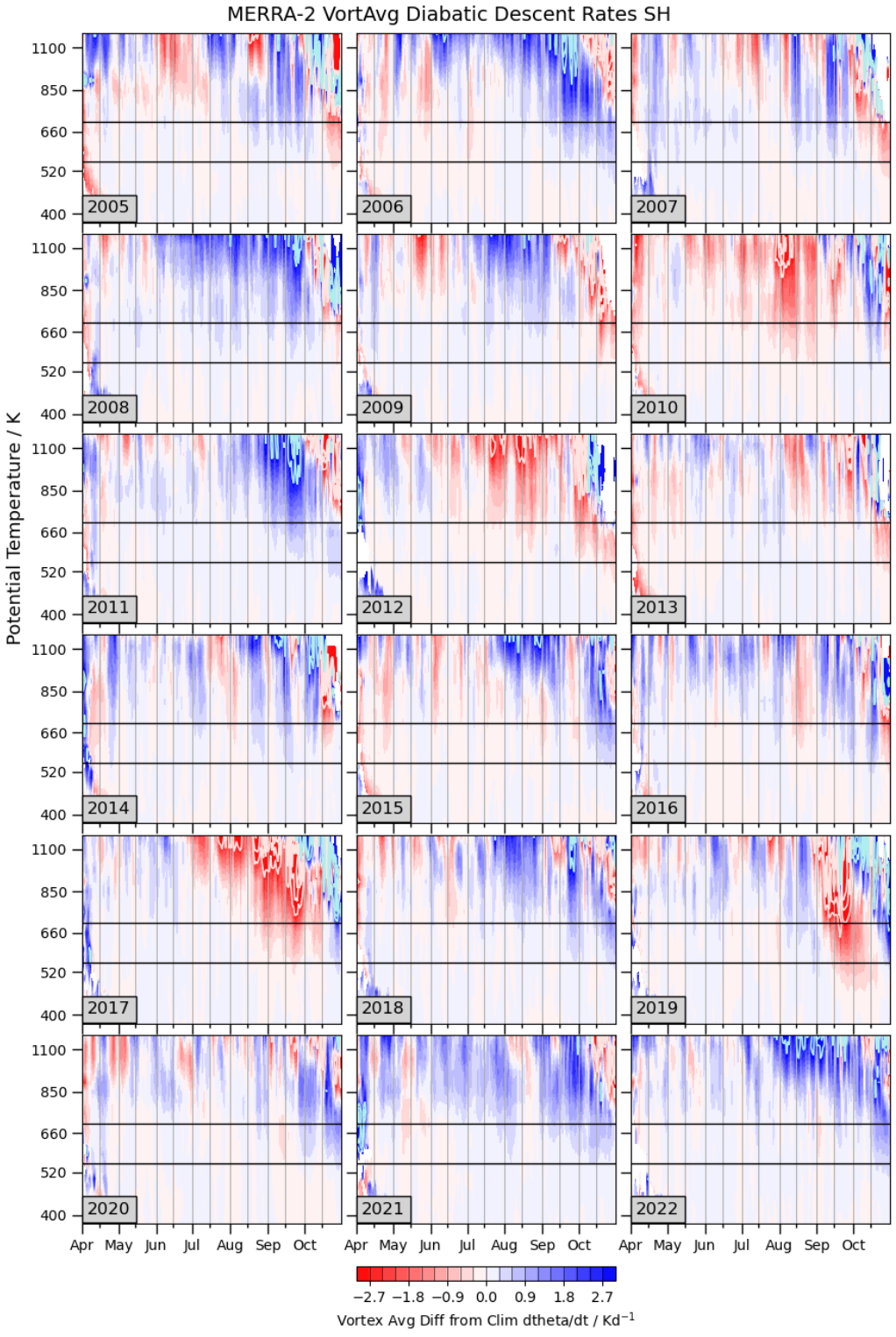

Figure S4. Cross-sections of anomalies from the 2005–2021 climatology of vortex-averaged diabatic heating/cooling rates from MERRA-2 for April through October in 2005 through 2022. Rates are expressed as dθ/dt. Up to three contours with an interval five times that shown in the colorbar are overlaid above the high value (cyan) and below the low value (pink) at which the color bar saturates. Overlaid horizontal lines mark 550 and 700 K. Note that the color scale has been inverted (negative values are reds) to emphasize anomalies indicating unusually strong descent.

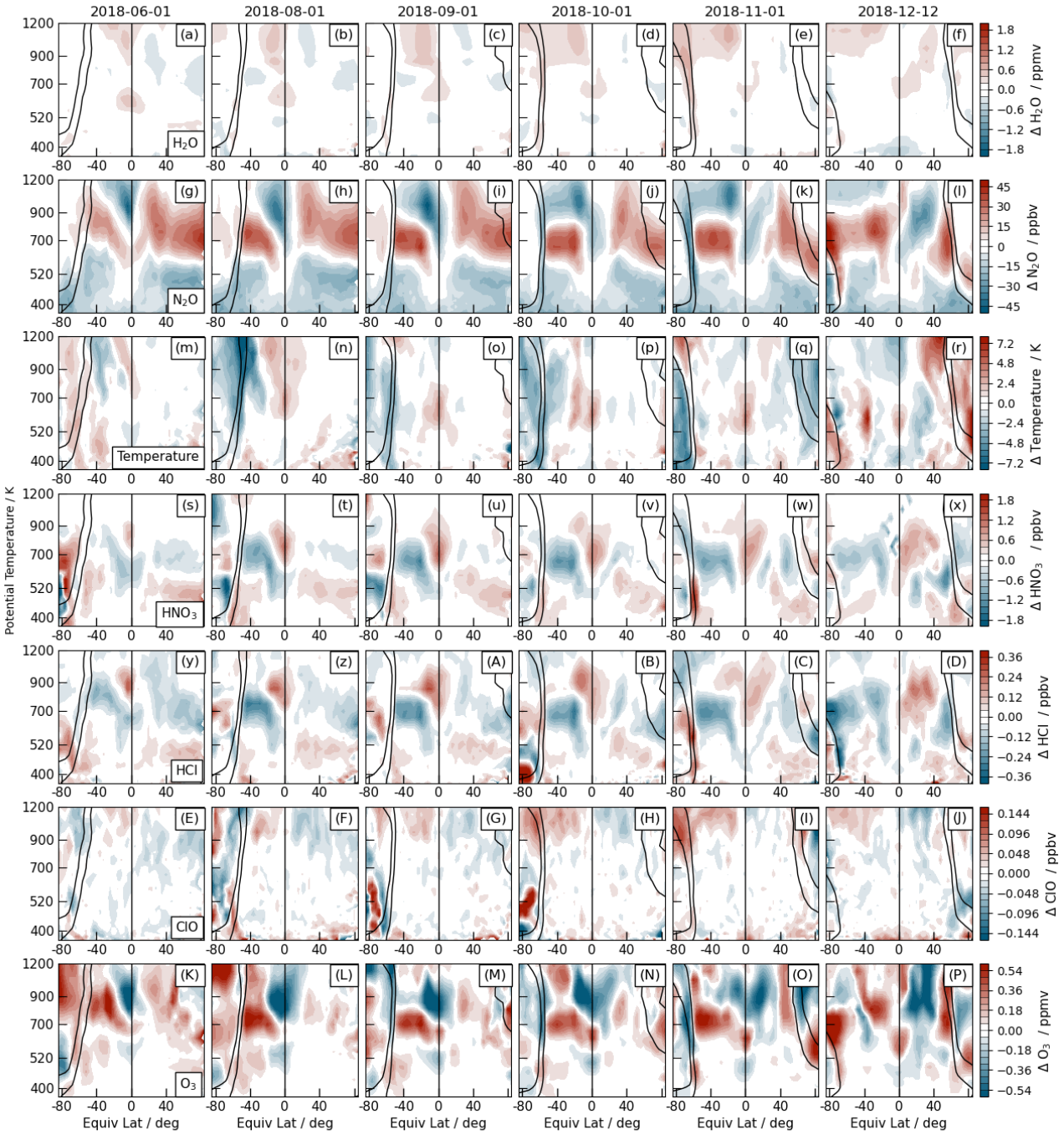

Figure S5. As in Fig. 3 in the main text, but for 2018: Snapshots on selected days in 2018 of anomalies from the 2005–2021 climatology of (top to bottom) MLS H_2O, N_2O, temperature, HNO_3, HCl, ClO, and O_3. Black overlaid contours are two contours of sPV representative of the vortex edge region.

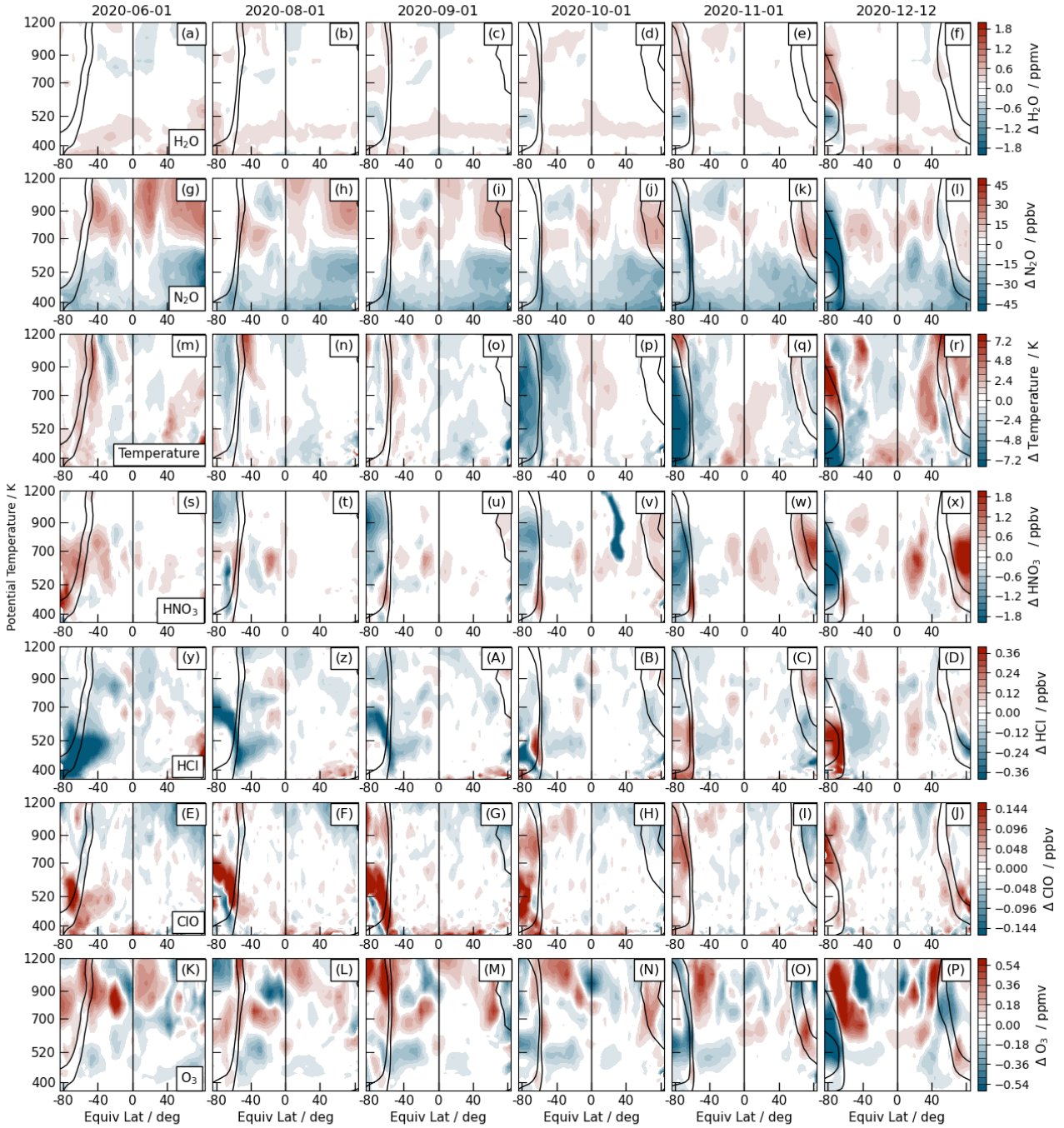

Figure S6. As in Fig. S5 but for 2020.

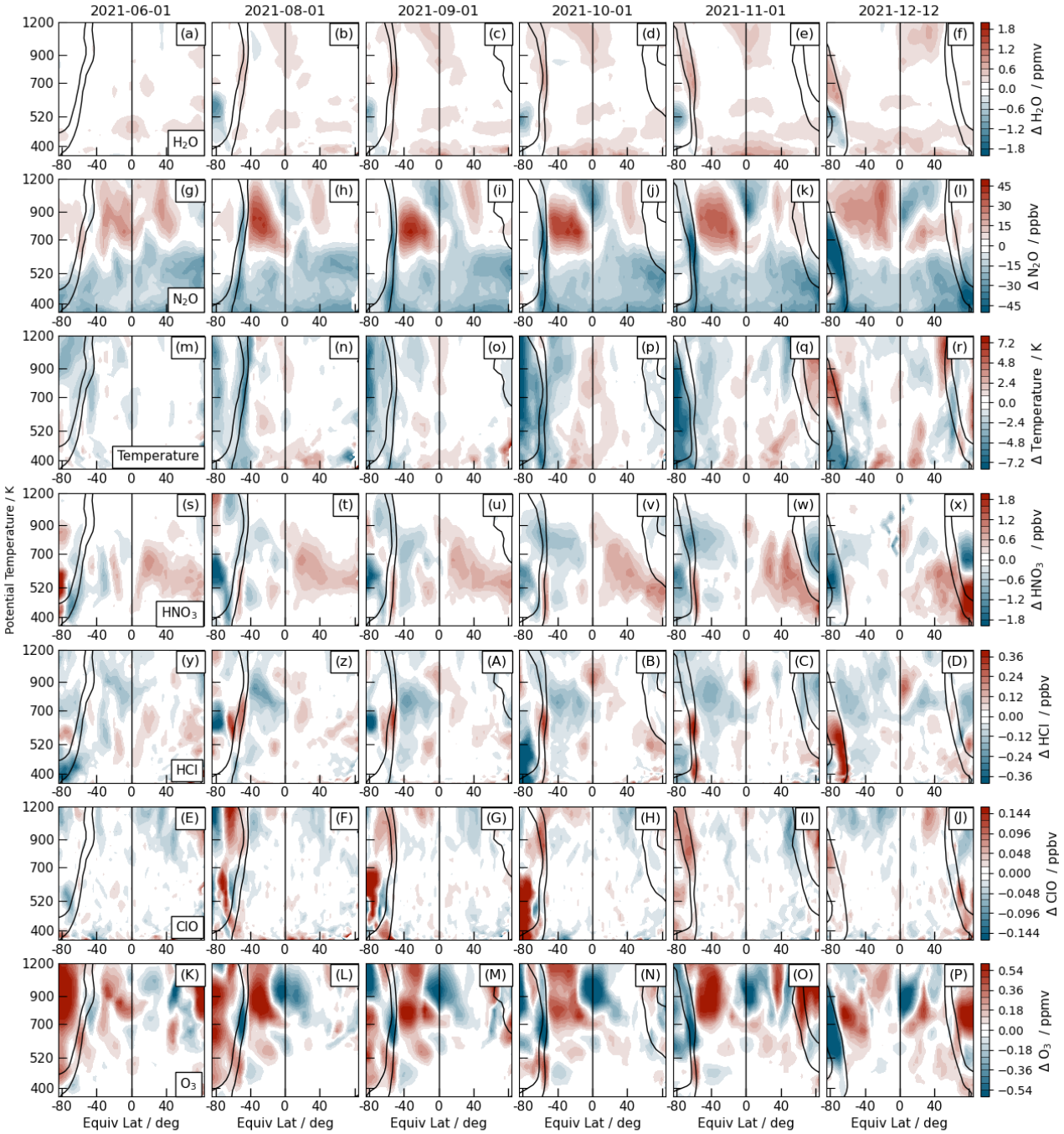

Figure S7. As in Fig. S5 but for 2021.

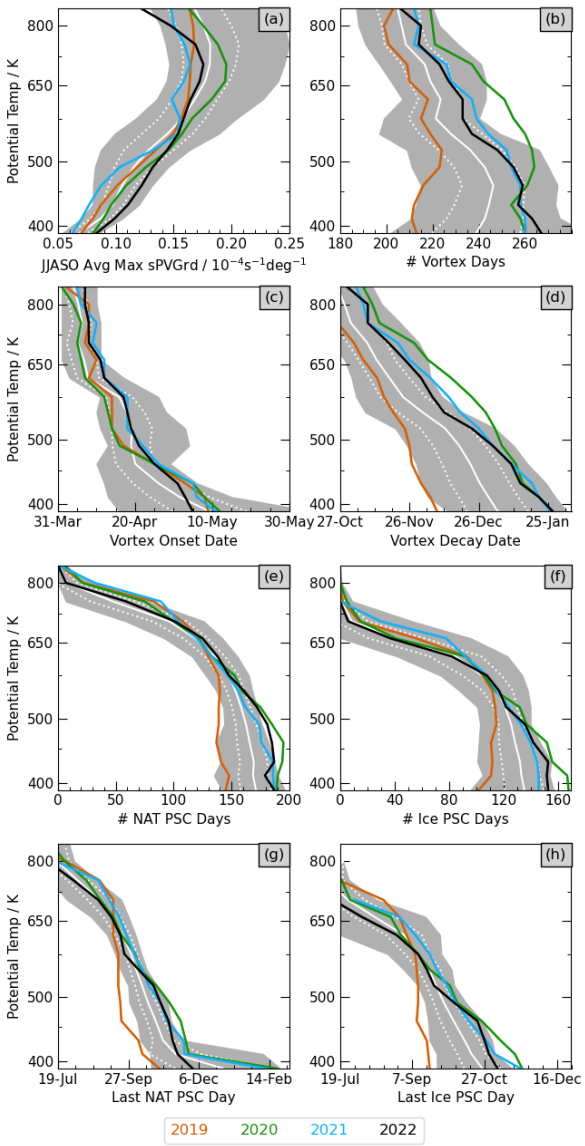

Figure S8. Profiles of summary vortex diagnostics calculated from MERRA-2 for 1979 through 2021 (excluding highlighted years). Highlighted years are 2019 (orange), 2020 (green), 2021 (cyan), and 2022 (black). Diagnostics are (left to right, top to bottom): June–October Average maximum sPV gradients; number of days when a vortex existed (defined as vortex area greater than 1% of a hemisphere); first date a vortex existed; last date a vortex existed; number of days with temperature less than the NAT PSC threshold; number of days with temperature less than the ice PSC threshold; last day temperatures were below the NAT PSC threshold; and last day temperatures were below the ice PSC threshold.

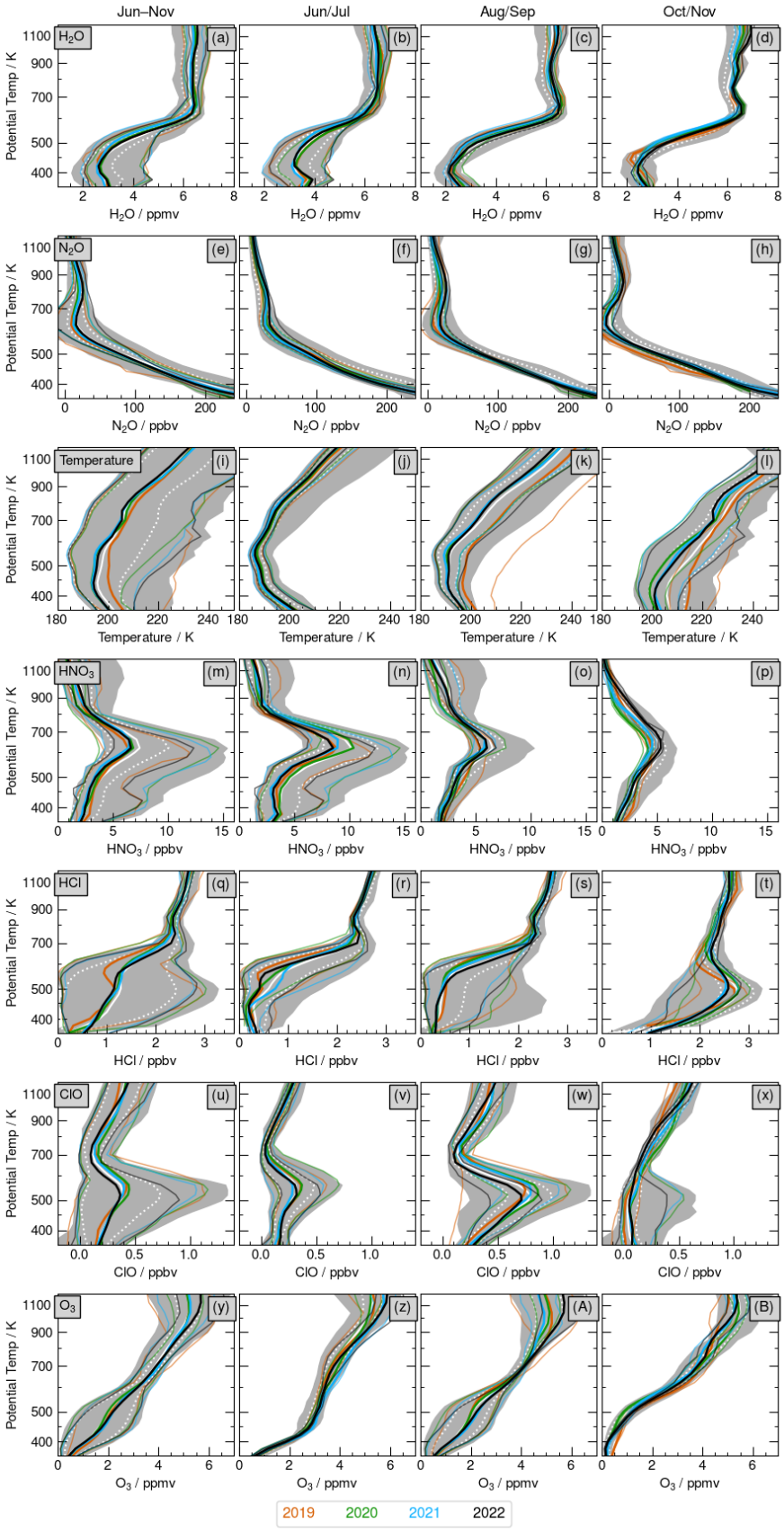

Figure S9. Profiles of vortex-averaged MLS data, averaged over (left to right) June through November; June/July; August/September; October/November. Fields shown are (top to bottom) H_2O, N_2O, temperature, HNO_3, HCl, ClO, and O_3. Grey envelope is the range excluding the highlighted years, and solid and dashed white lines are the mean and one standard deviation envelope for those years. Highlighted years are 2019 (orange), 2020 (green), 2021 (cyan), and 2022 (black).

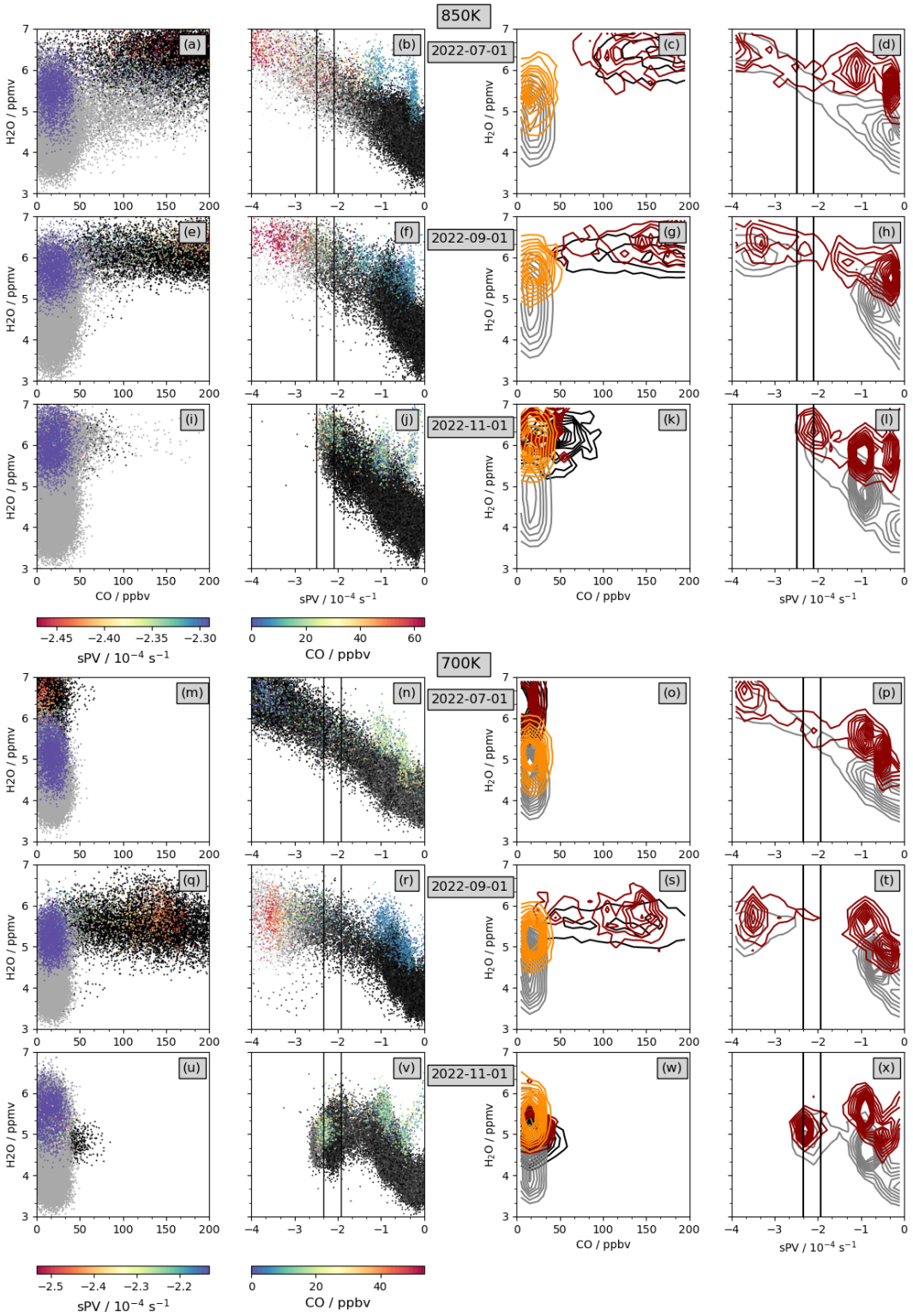

Figure S10. As in Fig. 5 in the main text, but for H_2O and sPV versus CO at 850 and 700 K: Scatter (left two columns) and density (right two columns) plots of MLS H_2O (y-axis) versus CO (first and third columns) and sPV (second and last columns). Grey and black dots (contours) show values from 2005–2021 in the scatter (density) plots; for those years, black (grey) indicates x-axis values of CO or sPV characteristic of inside (outside) the vortex. For 2022, colored (purple) dots or dark red (orange) contours show sPV values inside (outside) the vortex. 2022 CO (second column) is colored such that blue/blue-green shows typical vortex values. Black vertical lines on the plots versus sPV indicate the vortex edge region.

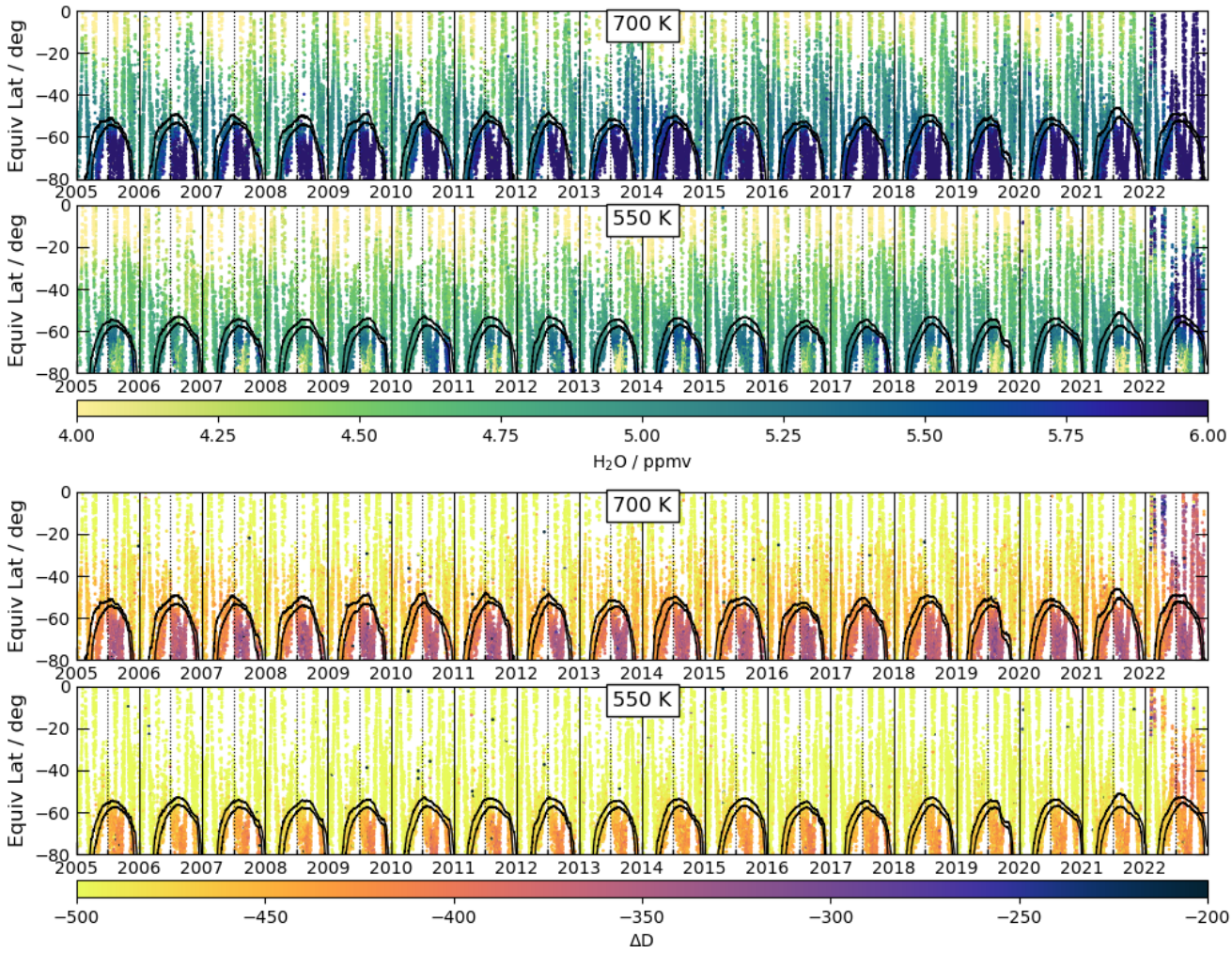

Figure S11. 700 and 550 K EqL/time plots of ACE-FTS H_2O and ΔD (HDO/H_2O, scaled as in Randel et al., 2012) for 2005–2022. Black overlays are sPV contours in the vortex edge region.

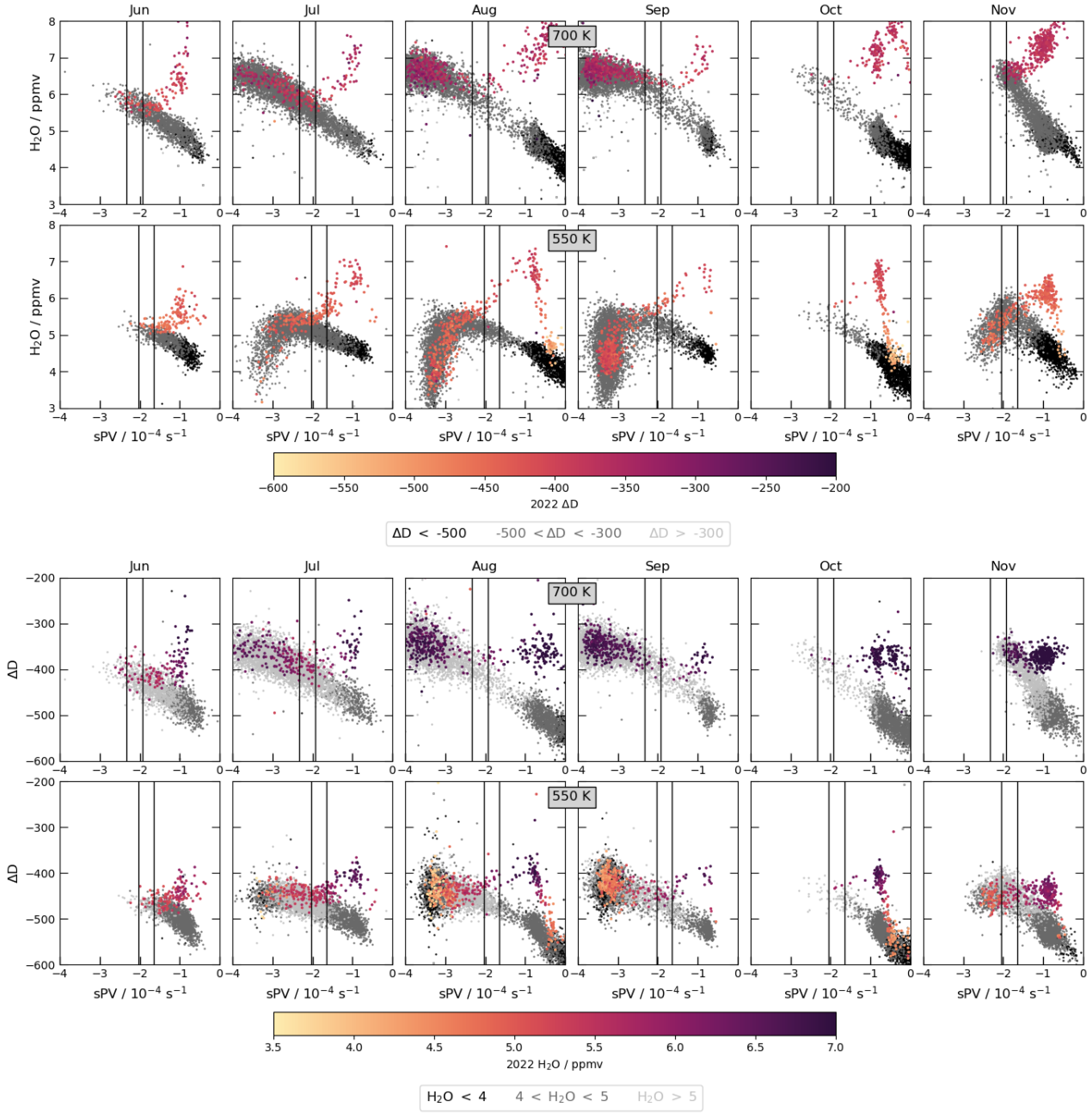

Figure S12. ACE-FTS H_2O and ΔD as a function of sPV, with 2022 values colored by ΔD and H_2O, respectively, and high, medium, and low values shown in black, grey, and pale grey, respectively, for preceding years from 2005 through 2021.